AAS 22-172

UNCERTAINTY ANALYSIS OF THE ELECTROSTATIC TRACTOR CONTROL PERFORMANCE

Julian Hammerl* **and Hanspeter Schaub†**

The electrostatic tractor concept is an active debris removal method that has been proposed to remove retired satellites from Geostationary Earth Orbit without physical contact, using electrostatic forces. These forces are generated by charging the servicing satellite and the debris with an electron gun that is attached to the servicer. Prior work investigated the effects of debris attitude on performance factors such as reorbit time and control effort. Uncertainty in the electric potential of the debris was also considered. This work extends the analysis of the electrostatic tractor performance by considering additional sources of uncertainty, such as uncertainty in mass properties, charge model errors, and electric potential uncertainty of the servicing satellite. The results suggest that errors in the estimated electric potential have the most significant impact on the reorbit performance.

INTRODUCTION

A number of methods have been proposed to relocate dysfunctional satellites from Geostationary Earth Orbit (GEO) to a graveyard orbit several hundred kilometers above GEO.[1,2] Some methods rely on a tether that connects the servicing spacecraft with the debris. A harpoon[3] or net[4] is attached to one end of the tether to capture the debris, while the other end of the tether is connected to the servicer. This allows the servicer to tug the debris to a different orbit. However, nets and harpoons might create new debris fragments upon impact, and using a tether is far from trivial and deserves its own area of space research.[5] Other methods aim at establishing a (approximately) rigid connection between the servicer and the debris, either by capturing the debris with robotic arms[6] or by docking with the debris.[7] However, high tumble rates[8,9] of retired satellites in GEO complicate these two approaches, as the relative rotation of the debris must either be matched by the servicer (at the cost of additional fuel), or the robotic arms must be capable of capturing a rotating object.[10]

The common theme of all aforementioned Active Debris Removal (ADR) methods is that they rely on physical contact. The Electrostatic Tractor (ET) has been proposed to touchlessly relocate retired satellites from GEO using electrostatic forces,[11,12] as illustrated in Fig. 1. A controlled servicing spacecraft is equipped with an electron gun that is aimed at the debris. Due to the emission of electrons, the servicer charges positively, while the debris charges negatively due to the accumulation of electrons. The resulting attractive electrostatic force acts as a virtual tether between the two spacecraft, allowing the servicer to tug the debris to a graveyard orbit using its low-thrust

*Graduate Research Assistant, Ann and H.J. Smead Department of Aerospace Engineering Sciences, University of Colorado Boulder, Colorado Center for Astrodynamics Research, Boulder, CO, 80303 USA. julian.hammerl@colorado.edu

†Professor, Glenn L. Murphy Chair of Engineering, Ann and H.J. Smead Department of Aerospace Engineering Sciences, University of Colorado Boulder, Colorado Center for Astrodynamics Research, Boulder, CO, 80303 USA. AAS Fellow, AIAA Fellow

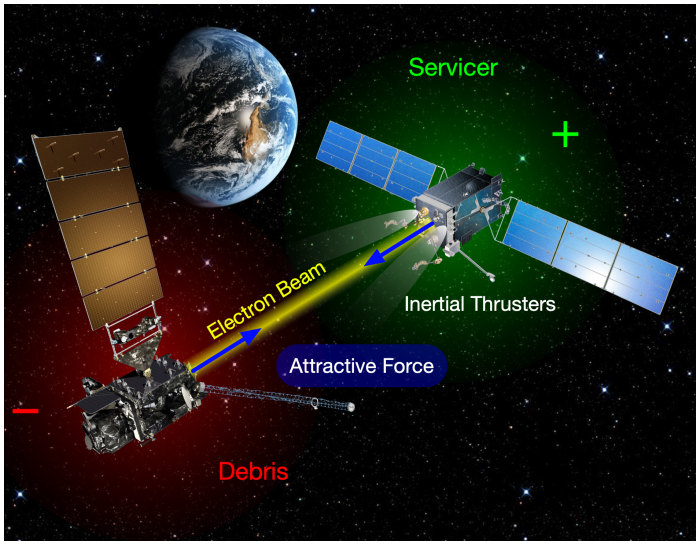

Figure 1: Electrostatic Tractor[13]

propulsion system. The touchless nature of the ET concept reduces the risk of generating additional debris fragments and makes it possible to relocate debris even if the debris is tumbling.

Prior work developed a relative motion control for the ET and showed that it is possible to raise the orbit altitude of the debris by 300 km within two months.[14] The authors also studied the effects of charge uncertainty on the control stability. However, only spherical spacecraft models were considered. More recent work uses the Multi-Sphere Method (MSM) to investigate the effects of debris electric potential uncertainty on the relative motion equilibria for general three-dimensional spacecraft shapes.[13] Reference 15 studies the effects of debris attitude on the control effort and reorbiting time, with and without uncertainty of the debris electric potential. However, other sources of uncertainty – such as navigation errors, charge approximation errors, etc. – and their effects on the control effort were neglected.

The effects of electric charge or potential uncertainty of the debris on the Electrostatic Tractor relative motion control have been studied in Refs. 13–15. However, uncertainty of the servicer potential is not considered in these studies. Reference 16 studies the effects of electrostatic force perturbations on proximity operations such as rendezvous and docking, and the authors propose a control that feeds forward on the estimated potentials and resulting forces and torques. The authors also investigate the sensitivity of the estimated force to the estimated potentials of the servicer and debris. Instead of considering the absolute debris potential estimation error, the error of the relative potential between the servicer and the debris is considered, because remote electric potential sensing methods that are being developed are only capable of estimating the relative potential.[17,18] The results of the study about electrostatic perturbations in Ref. 16 show that the estimated force is more sensitive to errors in the estimated servicer potential than the estimated relative potential, because the estimated absolute debris potential is a function of both the estimated servicer potential and the estimated relative potential.

The focus of this work is to compare the relative impact of different sources of uncertainty, such as electric potential uncertainty of the debris and the servicer, navigation errors, uncertainty in mass properties, and MSM model errors.

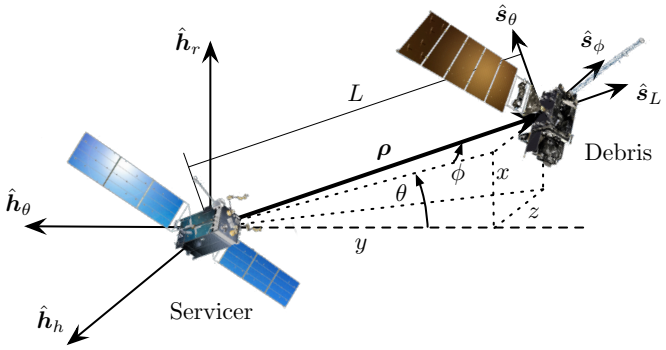

Figure 2: Hill frame $\mathcal{H}$ and Spherical frame $\mathcal{S}$[13]

PROBLEM STATEMENT

Relative Motion

The relative motion dynamics and control used for the Electrostatic Tractor are derived in Reference 14. Because the equations of motion are coupled in the Hill frame $\mathcal{H} : \{\hat{\boldsymbol{h}}_r, \hat{\boldsymbol{h}}_\theta, \hat{\boldsymbol{h}}_h\}$, a system of spherical coordinates (L, θ, ϕ) in the frame $\mathcal{S} : \{\hat{\boldsymbol{s}}_L, \hat{\boldsymbol{s}}_\theta, \hat{\boldsymbol{s}}_\phi\}$ is used for the relative motion control, as illustrated in Fig. 2. The feedback-control

$$^{\mathcal{S}}\boldsymbol{u} = [G(L,\phi)]^{-1}\Big(- [P]\dot{\boldsymbol{X}} - [K](\boldsymbol{X} - \boldsymbol{X}_r) - [\boldsymbol{F}(L,\theta,\phi,\dot{L},\dot{\theta},\dot{\phi})]\Big) \tag{1}$$

is globally asymptotically stabilizing,[14] where $\boldsymbol{X} = [L, \theta, \phi]^T$ is the state vector for the relative motion control, $\boldsymbol{X}_r$ is the desired state, $[K]$ and $[P]$ are feedback gain matrices, and $\boldsymbol{F}$ and $[G]$ include the equations of motion in the spherical frame $\mathcal{S}$. Diagonal gain matrices $[K]$ and $[P]$ are chosen with the same feedback gain K_L for all states, such that $[K] = K_L[I]_{3\times3}$ with identity matrix $[I]_{3\times3}$. For a slightly underdamped response the diagonal elements P_i of $[P]$ are determined by $P_i = 1.85\sqrt{K_i}$. The required thruster acceleration

$$\boldsymbol{u}_T = -\boldsymbol{u} - \boldsymbol{F}_{c,\text{est}}\left(\frac{1}{m_{T,\text{fsw}}} + \frac{1}{m_{D,\text{fsw}}}\right) \tag{2}$$

consists of the feedback control term $\boldsymbol{u}$ and a feed-forward term of the estimated electrostatic force $\boldsymbol{F}_{c,\text{est}}$ that is acting on the servicer. The mass of the servicer (tug, T) and the debris used by the flight software (the controller) are denoted by $m_{T,\text{fsw}}$ and $m_{D,\text{fsw}}$, respectively. Note that the expected mass used in the flight software can vary from the actual mass m_T and m_D used for the dynamics.

Rotational Dynamics

The electrostatic force also induces an electrostatic torque if the center of mass of an object does not align with its center of charge. Since the debris is uncontrolled, its attitude generally changes during the reorbit process as a result of the electrostatic torque. The rotational dynamics of the debris are given by [19, Chapter 4]

$$[I_D]\dot{\boldsymbol{\omega}} = -[\tilde{\boldsymbol{\omega}}][I_D]\boldsymbol{\omega} + \boldsymbol{L}_c \tag{3}$$

where $[I_D]$ is the inertia matrix of the debris, $\boldsymbol{\omega}$ is the angular velocity of the debris, and $\boldsymbol{L}_c$ is the electrostatic torque acting on the debris. The skew-symmetric matrix $[\tilde{\boldsymbol{\omega}}]$ is used as the cross-product equivalent matrix operator of $\boldsymbol{\omega}$. The inertia matrix and the location of the center of mass are obtained from a CAD model of the debris that is generated using publicly available size and mass information of a GOES-R satellite.[20] The attitude of the servicer is held constant at the desired orientation, so no rotational dynamics need to be implemented for the servicer.

Multi-Sphere Method

The Multi-Sphere Method (MSM) is implemented to calculate the electrostatic force and torque acting on each object. This method uses a number of spheres to approximate the charge distribution of complex-shaped objects. The voltage to charge relationship is

$$\begin{bmatrix} V_1 \\ V_2 \\ \vdots \\ V_n \end{bmatrix} = k_c \begin{bmatrix} 1/R_1 & 1/r_{1,2} & \cdots & 1/r_{1,n} \\ 1/r_{2,1} & 1/R_2 & \cdots & 1/r_{2,n} \\ \vdots & \vdots & \ddots & \vdots \\ 1/r_{n,1} & 1/r_{n,2} & \cdots & 1/R_n \end{bmatrix} \begin{bmatrix} Q_1 \\ Q_2 \\ \vdots \\ Q_n \end{bmatrix} \tag{4}$$

where V_i is the electric potential of the i-th sphere, R_i the radius, Q_i the electric charge, r_{ij} is the distance between the i-th and j-th sphere, and $k_c = 8.988 \times 10^9$ N m^2 / C^2 is the Coulomb constant. If the electric potential of each sphere is known, Eq. (4) is inverted to obtain the charge on each sphere, which is used to compute the electrostatic force and torque about generic point 0 acting on generic spacecraft 1 by

$$\boldsymbol{F}_1 = -k_c \sum_{j=1}^{n_1} \boldsymbol{Q}_{1_j} \left(\sum_{i=1}^{n_2} \frac{\boldsymbol{Q}_{2_i}}{r_{i,j}^3} \boldsymbol{r}_{i,j} \right) \tag{5}$$

and

$$\boldsymbol{L}_{1,0} = -k_c \sum_{j=1}^{n_1} \boldsymbol{r}_j \times \boldsymbol{Q}_{1_j} \left(\sum_{i=1}^{n_2} \frac{\boldsymbol{Q}_{2_i}}{r_{i,j}^3} \boldsymbol{r}_{i,j} \right) \tag{6}$$

where $\boldsymbol{r}_j$ is the vector from point 0 to the j-th sphere.

Spacecraft Models

Figure 3 shows the spacecraft models used in this analysis, as well as the corresponding (20 sphere) MSM models and reference frames. A GOES-R satellite is used to represent the debris due to its asymmetric shape resulting from the single solar panel and the magnetometer, and the servicer is based on an SSL-1300 satellite bus. The origin of the servicer frame $\mathcal{T} : \{\hat{\boldsymbol{t}}_1, \hat{\boldsymbol{t}}_2, \hat{\boldsymbol{t}}_3\}$ and of the debris frame $\mathcal{D} : \{\hat{\boldsymbol{d}}_1, \hat{\boldsymbol{d}}_2, \hat{\boldsymbol{d}}_3\}$ are located at the geometric center of the corresponding spacecraft. The nominal orientation of each spacecraft is defined as the orientation where the direction cosine matrix (DCM) that maps the Hill frame $\mathcal{H}$ into the corresponding spacecraft frame is equal to the identity matrix. In Fig. 3, both spacecraft are in their nominal orientation. A 3-1-2 (Yaw-Pitch-Rol) Euler Angle set is used to describe the orientation of each craft.

Simulation Setup

Both satellites start in GEO, and the servicer begins at its desired position $\boldsymbol{X} = \boldsymbol{X}_r = [20\,\text{m}, 0, 0]^T$. The debris is then reorbited to a graveyard orbit. The simulation parameters are shown in Tab. 1, where the difference in semi-major axis between the graveyard orbit and GEO is denoted by Δa,

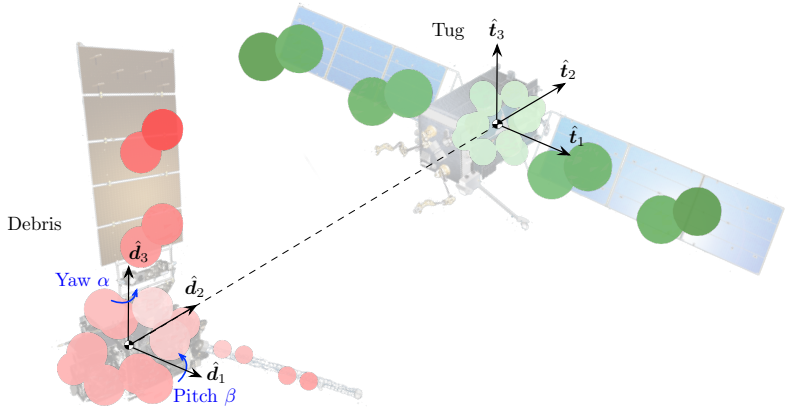

Figure 3: MSM Spacecraft models and spacecraft reference frames. The color of the MSM spheres indicates the electric charge: green corresponds to positive charge and red corresponds to negative charge; the stronger the color, the greater the charge magnitude[15]

Table 1: Simulation Parameters

m_T	m_D	Φ_T	Φ_D	L_r	Δa
2000 kg	2857 kg	25 kV	-25 kV	20 m	300 km

and the electric potentials of the tug and the debris are denoted by Φ_T and Φ_D, respectively. Fully conducting spacecraft are assumed, so all spheres have the the same electric potential as the corresponding spacecraft. While the attitude of the servicer is held constant at its nominal orientation, the debris is free to rotate according to the rotational dynamics in Eq. (3).

The *Basilisk* astrodynamics simulation framework is used for all simulations,[21] as it is capable of computing the electrostatic forces between several spacecraft using the Multi-Sphere Method.

UNCERTAINTY OF INDIVIDUAL FACTORS

For the following simulations, the debris starts with its nominal orientation and an angular velocity of 1 deg/s about the $\hat{\boldsymbol{\omega}}_{D/N} = [0.267, 0.535, 0.802]^T$ unit direction. A feedback gain of $K_L = 1 \cdot 10^{-6}$ is used.

Electric Potential

An electric potential estimation error for the servicer

$$\Delta\Phi_T = \Phi_{T,\text{est}} - \Phi_T \tag{7}$$

is applied, where $\Phi_{T,\text{est}}$ is the estimated potential of the servicer. For the debris, the error of the relative potential between the debris and the servicer

$$\Delta\Phi_{D,\text{rel}} = \Phi_{D,\text{rel,est}} - \Phi_{D,\text{rel}} = (\Phi_{D,\text{est}} - \Phi_{T,\text{est}}) - (\Phi_D - \Phi_T) \tag{8}$$

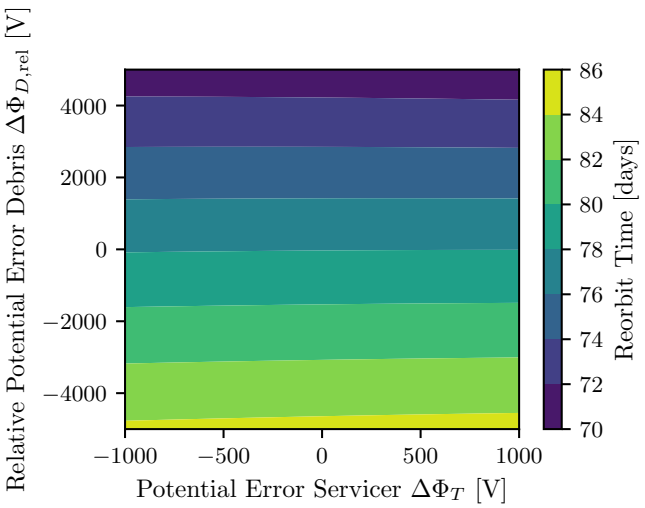

Figure 4: Reorbit Time for 300 km altitude raise as a function of potential estimation errors

is used, because remote electric potential sensing methods that are being developed are only capable of estimating the relative potential.[17,18] Consequently, the estimated absolute potential of the debris

$$\Phi_{D,\text{est}} = \Phi_{T,\text{est}} + \Phi_{D,\text{rel,est}} \tag{9}$$

also depends on the estimated potential of the servicer.

Figure 4 shows the reorbit time for a semi-major axis raise of 300 km as a function of the servicer and debris potential estimation errors. The reorbit time decreases with negative servicer potential errors and positive debris potential errors. Because the actual debris potential $\Phi_D = -25$ kV is negative, a positive debris potential error results in a smaller magnitude of the estimated potential. Consequently, the flight software under-predicts the electrostatic force and the servicer comes closer to the debris than the desired separation distance of $L_r = 20$ m, as investigated thoroughly in Ref. 13. As the electrostatic force magnitude decreases with $1/r^2$, the smaller separation distance causes a larger electrostatic force. To maintain the separation distance and avoid a collision, the relative motion controller has to compensate for the stronger attractive force by applying a greater thrust in the opposite direction, which decreases the reorbit time. The servicer potential $\Phi_T = 25$ kV, on the other hand, is positive. In this case, a negative potential error results in an under-prediction of the electrostatic force and a decrease in reorbit time due to the reasons explained above.

Interestingly, the estimated relative debris potential affects the reorbit time more than the estimated servicer potential. This seems to directly contradict the results found in Ref. 16, which show that the servicer potential error affects the estimated electrostatic force more than the relative debris potential error. However, that study deals with electrostatic perturbations on the relative motion, where both spacecraft are charged to equal sign and the electrostatic force is repulsive. This current analysis deals with attractive electrostatic forces. Reference 16 derives the sensitivity ratio of the (estimated) electrostatic force between two spheres to errors in the electric potentials

$$\frac{\partial F/\partial \Phi_T}{\partial F/\partial \Phi_{D,\text{rel}}} = \frac{(2\Phi_T + \Phi_{D,\text{rel}})(r^2 + R_T R_D) - 2R_T \Phi_T r - 2R_D r(\Phi_T + \Phi_{D,\text{rel}})}{\Phi_T(r^2 + R_T R_D) - 2R_D r(\Phi_T + \Phi_{D,\text{rel}})} \tag{10}$$

where r is the separation distance between the two spheres, R_T and R_D are the radii of the spheres, and Φ_T and $\Phi_{D,\text{rel}}$ are the absolute potential of the servicer sphere and relative potential of the debris

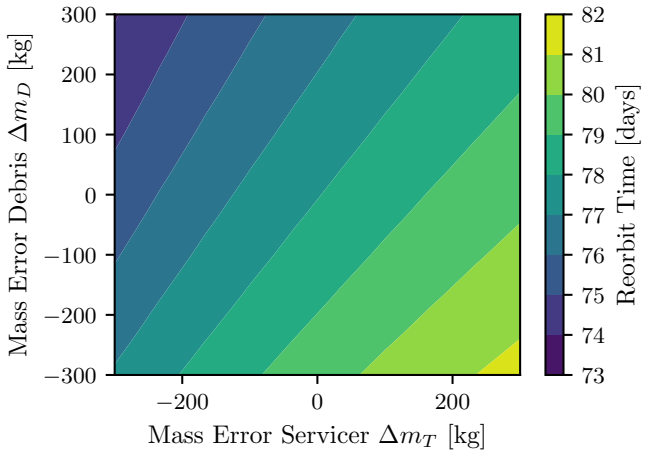

Figure 5: Reorbit Time for 300 km altitude raise as a function of mass errors

sphere, respectively. If both spheres are charged to the same potential ($\Phi_{D,\text{rel}} = 0$), the repulsive electrostatic force is more sensitive to errors in the servicer potential Φ_T. This is the case in Ref. 16. On the other hand, if $\Phi_T = 25$ kV and $\Phi_{D,\text{rel}} = -50$ kV, as it is the case in the current analysis, then the magnitude of the sensitivity ratio is less than 1, indicating that the force is more sensitive to errors in the relative potential $\Phi_{D,\text{rel}}$. Consequently, the reorbit time is also more affected by the relative debris potential.

Mass Properties

The mass of the two spacecraft might not be perfectly known. While the mass of the controlled servicing spacecraft is likely well known with errors of a few kilograms, the mass of the debris is much more uncertain. The dry mass of the targeted retired satellite provides a good estimate for its mass, but the actual mass can vary greatly, especially if parts of the satellite have fallen off.

Figure 5 shows the effects of mass errors on the reorbit time, where the mass error of the servicer

$$\Delta m_T = m_{T,\text{fsw}} - m_T \tag{11}$$

is the difference between the expected servicer mass $m_{T,\text{fsw}}$ used by the flight software (i.e. the controller) and the actual mass of the servicer m_T. Similarly, the mass error of the debris is defined as

$$\Delta m_D = m_{D,\text{fsw}} - m_D \tag{12}$$

The results show that a positive error Δm_T increases the reorbit time while a positive error Δm_D decreases the reorbit time. From the required thruster acceleration in Eq. (2), one can compute the necessary thrust that the controller commands

$$\boldsymbol{T}_T = m_{T,\text{fsw}} \cdot \boldsymbol{u}_T = -m_{T,\text{fsw}}\boldsymbol{u} - \boldsymbol{F}_{c,\text{est}}\left(1 + \frac{m_{T,\text{fsw}}}{m_{D,\text{fsw}}}\right) \tag{13}$$

Essentially, a larger $m_{T,\text{fsw}}$ (due to a positive Δm_T) corresponds to an over-prediction of the acceleration due to the electrostatic force, while a larger $m_{D,\text{fsw}}$ corresponds to an under-prediction. As described in the previous section, an over-prediction of the force leads to an increase in reorbit time, while an under-prediction reduces the time.

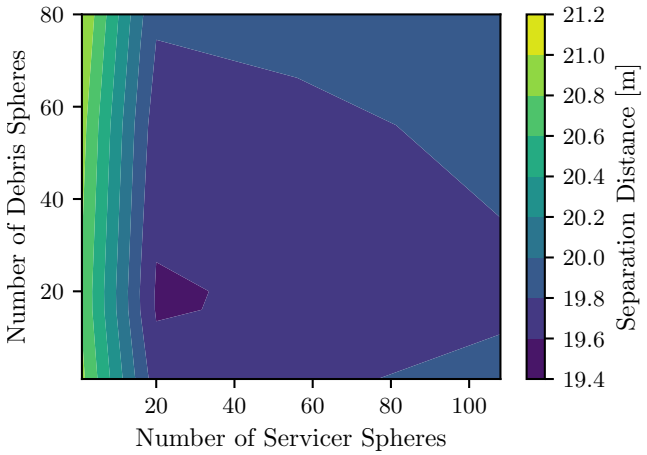

Figure 6: Average separation distance during 300 km altitude raise as a function of MSM model spheres

MSM Model Errors

While the Multi-Sphere Method provides a good approximation of the charge distribution of the two-craft formation, it cannot replicate the actual charge distribution perfectly. The effect of such model errors is simulated by using a high fidelity MSM model for the dynamics part in Basilisk, while the flight software in Basilisk uses a lower fidelity MSM model. In other words, the estimated electrostatic force used by the controller is computed using MSM models with a smaller number of spheres, while the actual electrostatic force that is used for the dynamics propagation is computed with MSM models with a higher number of spheres. The higher fidelity model for the dynamics part uses 108 spheres for the servicer and 80 spheres for the debris, and the number of spheres used by the flight software is varied.

The average separation distance between the two spacecraft during the reorbit process as a function of the number of MSM model spheres is shown in Fig. 6. If the flight software and dynamics MSM models are identical (108 servicer spheres and 80 debris spheres), then the average separation distance is 20 m, which corresponds to the desired separation distance L_r. With a lower fidelity model, the average separation distance generally deviates from the desired 20 m, but all multi-sphere models perform reasonably well. The lowest fidelity multi-sphere model uses 16 spheres on each spacecraft. For the simplest model, which uses a single sphere to represent each craft, the average separation distance is about 21 m. Interestingly, if only one sphere is used for the servicer, the number of debris spheres does not seem to impact the separation distance significantly. This is likely due to the debris spinning with 1 deg/s. The orientation of the debris has a significant effect on the electrostatic force between the two spacecraft, but if the debris is spinning, then the electrostatic force is averaged over time.[15] Thus, for a spinning debris, the number of spheres on the debris is not crucial.

Feedback Gain Selection

For all previous simulations, a feedback gain of $K_L = 1 \cdot 10^{-6}$ is used. The relation between the feedback gain and the resulting Delta-V is studied in this section. Navigation errors are included for the servicer spacecraft according to Tab. 2. No navigation errors larger than the error bounds are

Table 2: Navigation Error Parameters

Position Std. Dev.	Velocity Std. Dev.	Position Error Bound	Velocity Error Bound
$1 \cdot 10^{-2}$ m	$1 \cdot 10^{-4}$ m/s	$5 \cdot 10^{-1}$ m	$5 \cdot 10^{-3}$ m/s

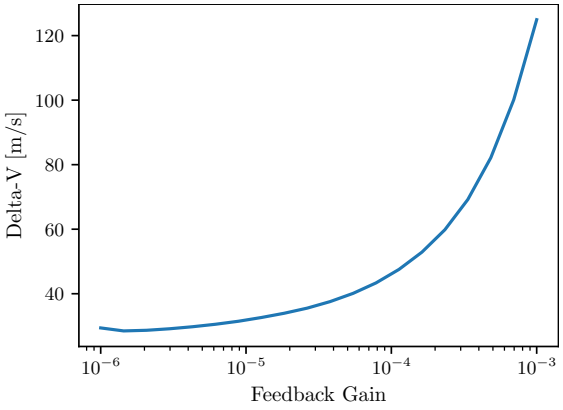

Figure 7: Delta-V vs. Feedback Gain

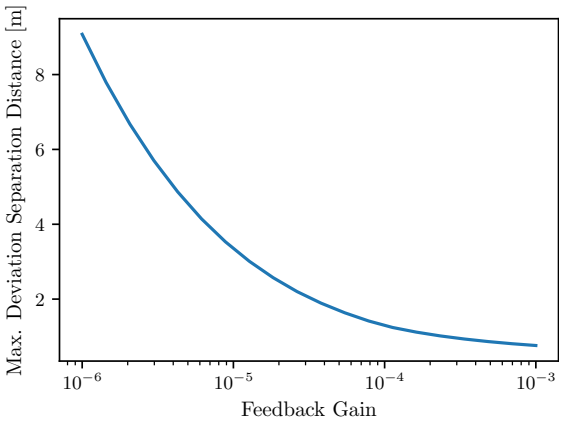

Figure 8: Max. Deviation vs. Feedback Gain

applied, and the same standard deviation and error bound is used for all directions.

Figure 7 shows the effect of the feedback gain on Delta-V, where the Delta-V is computed by

$$\Delta V = \int |\boldsymbol{u}_T| \, \mathrm{d}t \tag{14}$$

and Fig. 8 shows the maximum deviation from the desired separation distance of 20 m during the reorbit process. As expected, a higher feedback gain K_L reduces the deviation from the desired position, but at the cost of increased Delta-V. In addition to reducing the effects of navigation errors, a higher feedback gain also reduces the impact of potential estimation errors and mass errors. However, this results in Delta-Vs approaching 100 m/s. On the other hand, a low feedback gain increases the deviation from the desired separation distance significantly. For a deviation of 6 m, the servicer comes dangerously close to the debris, which could cause a collision with the 10 m long solar panel of the debris, especially if the debris is tumbling. Given these results, a feedback gain of $K_L = 1 \cdot 10^{-5}$ is chosen for the following Monte Carlo simulation.

MONTE CARLO SIMULATION

A Monte Carlo simulation of the reorbit process is performed with 100 runs. The potential estimation errors and mass errors are dispersed according to Tab. 3, where $\mathcal{N}(\mu, \sigma^2)$ denotes a normal distribution with mean μ and standard deviation σ. The initial orientation and rotation is also randomized, with a bound of 2 deg/s for the initial angular velocity. Navigation errors are applied according to Tab. 2.

Figures 9 and 10 show the histograms of the reorbit time and Delta-V during the 300 km altitude raise reorbit process. The mean reorbit time is 67.7 days with a standard deviation of 9.5 days, and the mean Delta-V is 31.5 m/s with a standard deviation of 1.2 m/s. Figure 11 shows the separation

Table 3: Dispersions

$\Delta\Phi_{D,\text{rel}}$ [V]	$\Delta\Phi_T$ [V]	Δm_D [kg]	Δm_T [kg]
$\mathcal{N}(0, 1000^2)$	$\mathcal{N}(0, 300^2)$	$\mathcal{N}(0, 50^2)$	$\mathcal{N}(0, 3^2)$

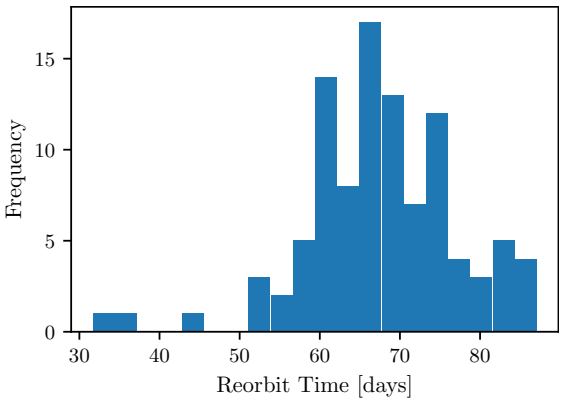

Figure 9: Histogram of Reorbit Times

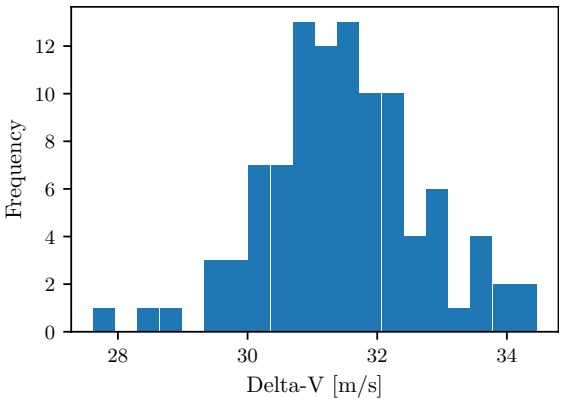

Figure 10: Histogram of Delta-V

distance as a function of time for one day and 5 of the 100 Monte Carlo runs. The separation distances chatter around 20 m, suggesting that there is no significant offset in the equilibrium position due to errors in the estimated potential or expected mass. Thus, for the given feedback gain and navigation error parameters, the navigation errors dominate the impact on the control performance. However, this is mainly due to the tumbling debris. As shown in Ref. 15, a tumbling debris decreases the effect of potential estimation errors. If the orientation of the debris is held constant using remote electrostatic attitude control concepts,[22] then the effect of electric potential errors on the control performance increases.

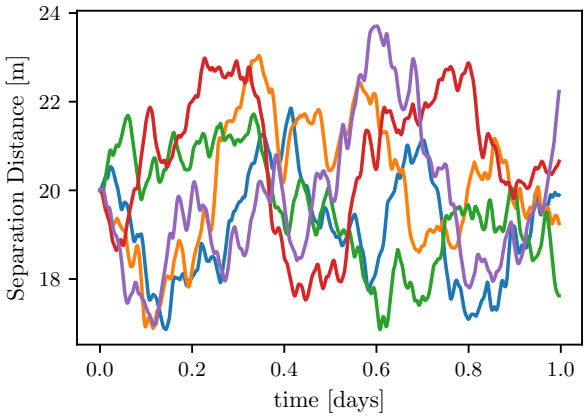

Figure 11: Separation distance for 5 of the 100 Monte Carlo runs

CONCLUSIONS

This paper investigates the effects of different sources of uncertainty and modeling errors on the reorbit time and Delta-V requirement of the Electrostatic Tractor debris reorbit process. Sources of uncertainty include electric potential estimation errors, uncertainty in the expected mass of each satellite, and navigation errors. Multi-Sphere models of lower fidelity are also included in the flight software, while the dynamics are propagated using a higher fidelity model. The results suggest that, for the magnitude of errors used in this work, electric potential errors affect the performance more than uncertainty in the spacecraft mass, due to the direct relationship of electric potential errors on the electrostatic force between the two satellites. Interestingly, for the Electrostatic Tractor, the estimated electrostatic force is more sensitive to errors in the estimated relative potential between debris and servicer than to errors of the servicer potential. While lower fidelity Multi-Sphere models in the flight software (for the estimation of the electrostatic force) only marginally affect the reorbit process, single-sphere models have a more noticeable effect. A high enough feedback gain must be selected such that the controller can withstand uncertainty in the electric potentials and navigation errors.

ACKNOWLEDGMENTS

This work was supported by U.S. Air Force Office of Scientific Research under grant FA9550-20-1-0025.

REFERENCES

[1] M. Shan, J. Guo, and E. Gill, "Review and comparison of active space debris capturing and removal methods," *Progress in Aerospace Sciences*, Vol. 80, jan 2016, pp. 18–32, 10.1016/j.paerosci.2015.11.001.

[2] C. P. Mark and S. Kamath, "Review of Active Space Debris Removal Methods," *Space Policy*, Vol. 47, feb 2019, pp. 194–206, 10.1016/j.spacepol.2018.12.005.

[3] R. Dudziak, S. Tuttle, and S. Barraclough, "Harpoon technology development for the active removal of space debris," *Advances in Space Research*, Vol. 56, aug 2015, pp. 509–527, 10.1016/j.asr.2015.04.012.

[4] M. Shan, J. Guo, and E. Gill, "Deployment dynamics of tethered-net for space debris removal," *Acta Astronautica*, Vol. 132, mar 2017, pp. 293–302, 10.1016/j.actaastro.2017.01.001.

[5] M. P. Cartmell and D. J. McKenzie, "A review of space tether research," *Progress in Aerospace Sciences*, Vol. 44, No. 1, 2008, pp. 1–21, 10.1016/j.paerosci.2007.08.002.

[6] D. Reintsema, J. Thaeter, A. Rathke, W. Naumann, P. Rank, J. Sommer, and K.-T. GmbH, "DEOS – The German Robotics Approach to Secure and De-Orbit Malfunctioned Satellites from Low Earth Orbits," *10th International Symposium on Artificial Intelligence, Robotics and Automation in Space (i-SAIRAS'10)*, Sapporo, Japan, aug 2010, pp. 244–251.

[7] C. Blackerby, A. Okamoto, S. Iizuka, Y. Kobayashi, K. Fujimoto, Y. Seto, S. Fujita, T. Iwai, N. Okada, J. Forshaw, and A. Bradford, "The ELSA-d end-of-life debris removal mission: Preparing for launch," *Proceedings of the International Astronautical Congress, IAC*, Washington DC, International Astronautical Federation; Paris, France, oct 2019, pp. 1–8.

[8] J. Šilha, J.-N. Pittet, M. Hamara, and T. Schildknecht, "Apparent rotation properties of space debris extracted from photometric measurements," *Advances in Space Research*, Vol. 61, feb 2018, pp. 844–861, 10.1016/j.asr.2017.10.048.

[9] P. Papushev, Y. Karavaev, and M. Mishina, "Investigations of the evolution of optical characteristics and dynamics of proper rotation of uncontrolled geostationary artificial satellites," *Advances in Space Research*, Vol. 43, may 2009, pp. 1416–1422, 10.1016/j.asr.2009.02.007.

[10] S.-I. Nishida and S. Kawamoto, "Strategy for capturing of a tumbling space debris," *Acta Astronautica*, Vol. 68, jan 2011, pp. 113–120, 10.1016/j.actaastro.2010.06.045.

[11] H. Schaub and D. F. Moorer, "Geosynchronous Large Debris Reorbiter: Challenges and Prospects," *The Journal of the Astronautical Sciences*, Vol. 59, jun 2012, pp. 161–176, 10.1007/s40295-013-0011-8.

[12] M. Bengtson, K. Wilson, J. Hughes, and H. Schaub, "Survey of the electrostatic tractor research for reorbiting passive GEO space objects," *Astrodynamics*, Vol. 2, dec 2018, pp. 291–305, 10.1007/s42064-018-0030-0.

[13] J. Hammerl and H. Schaub, "Effects of Electric Potential Uncertainty on Electrostatic Tractor Relative Motion Control Equilibria," *Journal of Spacecraft and Rockets*, sep 2021, pp. 1–11. in press, 10.2514/1.A35165.

[14] E. A. Hogan and H. Schaub, "Relative Motion Control For Two-Spacecraft Electrostatic Orbit Corrections," *Journal of Guidance, Control, and Dynamics*, Vol. 36, jan 2013, pp. 240–249, 10.2514/1.56118.

[15] J. Hammerl and H. Schaub, "Debris Attitude Effects on Electrostatic Tractor Relative Motion Control Performance," *AAS/AIAA Astrodynamics Specialist Conference*, Big Sky, MT, aug 2021, pp. 1–13.

[16] K. Wilson and H. Schaub, "Constrained guidance for spacecraft proximity operations under electrostatic perturbations," *IEEE Aerospace Engineering Conference*, Big Sky, MT, mar 2021, pp. 1–11.

[17] M. Bengtson, J. Hughes, and H. Schaub, "Prospects and Challenges for Touchless Sensing of Spacecraft Electrostatic Potential Using Electrons," *IEEE Transactions on Plasma Science*, Vol. 47, aug 2019, pp. 3673–3681, 10.1109/TPS.2019.2912057.

[18] K. Wilson and H. Schaub, "X-Ray Spectroscopy for Electrostatic Potential and Material Determination of Space Objects," *IEEE Transactions on Plasma Science*, Vol. 47, aug 2019, pp. 3858–3866, 10.1109/TPS.2019.2910576.

[19] H. Schaub and J. L. Junkins, *Analytical Mechanics of Space Systems*. Reston, VA: AIAA Education Series, 4th ed., 2018, 10.2514/4.105210.

[20] K. T. H. Wilson, *Remote Electrostatic Potential Determination for Spacecraft Relative Motion Control*. Doctoral thesis, University of Colorado Boulder, 2021.

[21] P. W. Kenneally, S. Piggott, and H. Schaub, "Basilisk: A flexible, scalable and modular astrodynamics simulation framework," *Journal of Aerospace Information Systems*, Vol. 17, No. 9, 2020, pp. 496–507, 10.2514/1.I010762.

[22] D. Stevenson and H. Schaub, "Electrostatic spacecraft rate and attitude control—Experimental results and performance considerations," *Acta Astronautica*, Vol. 119, feb 2016, pp. 22–33, 10.1016/j.actaastro.2015.10.023.